A continuous-wave vortex Raman laser with sum frequency generation

Andrew J. Lee[1] · Helen M. Pask[1] · Takashige Omatsu[2]

Abstract Sum frequency generation of the fundamental and Stokes fields within an intracavity self-Raman vortex laser is demonstrated in a linear resonator configuration. In this system, the sum frequency field exhibits different spatial profiles in the near and far fields, and a time-varying topological charge which varies between values of $+2$ and 0. We present a theoretical model which supports these experimental observations.

1 Introduction

Vortex laser beams have seen use across a wide range of applications including optical manipulation [1], quantum information [2], materials processing [3–5], and ultra-resolution microscopy [6]. The diversity of these applications stems from the unique properties of vortex beams, particularly their annular profile, and orbital angular momentum [2, 7]. In the interest of further increasing the versatility of vortex laser beams, it is necessary to improve the range of wavelengths that can be generated from vortex laser sources, and also, to exercise control over the topological charge of the vortex beam and its spatial profile (in particular, the size of the central null region).

A Gaussian laser beam can be converted to a vortex beam using external components such as spiral phase plates [8]

and spatial light modulators [9]. These components also enable control of the topological charge of the resultant vortex beam. However, the beam quality and power scaling capacity of these sources may be limited by damage and diffraction loss to these external components. An alternative method of directly generating a vortex laser beam, which foregoes the use of potentially fragile external elements, is to suppress oscillation of the lowest-order Gaussian mode within a laser cavity and instead force oscillation of a Laguerre–Gaussian (LG) mode (LG_{0x} modes are vortex modes with topological charge x) [10]. This can be performed in a number of ways, including using an on-axis damage spot [11, 12], utilizing soft aperture effects owing to thermal lensing [13], or by controlling the gain profile within the laser [14]. By forcing the laser to oscillate on a different cavity mode, many of the desirable properties of the laser are retained, including power scalability and beam quality; also system simplicity is retained with no alignment of external optics.

A number of groups have demonstrated methods of increasing the wavelength diversity of vortex lasers through nonlinear conversion processes such as second-harmonic generation (SHG) [15–17], optical parametric oscillation (OPOs) [18, 19], difference frequency generation [20], and stimulated Raman scattering (SRS) [12]. We recently demonstrated the simultaneous application of intracavity SRS and SHG to produce vortex laser emission at 586 nm from a self-Raman laser [21]. This laser generated three vortex beams at different wavelengths: two in the near infrared (NIR) at 1063 and 1173 nm and one in the visible at 586 nm. In that work, we demonstrated that orbital angular momentum is conserved under processes of SRS and SHG, wherein the topological charge of the fundamental field is transferred to the Stokes field under SRS (sign of the topological charge was also maintained), and summation of the topological charge occurs under SHG.

✉ Andrew J. Lee
andrew.lee@mq.edu.au

[1] Department of Physics and Astronomy, MQ Photonics Research Centre, Macquarie University, Sydney, NSW 2109, Australia

[2] Graduate School of Advanced Integration Science, Chiba University, Chiba 263 8522, Japan

In this work, we examine, in detail, the process of sum frequency generation (SFG) of fundamental and Stokes laser modes within a self-Raman vortex laser. In contrast to the case of SHG in which one optical field (for example the Stokes) gives rise to another, SFG involves the nonlinear mixing of two different fields, in this case, the Stokes and fundamental. Hence, the properties of each of these fields influence the resultant SFG output, resulting in more complex behaviour.

2 Experiment

The layout of the laser resonator is shown schematically in Fig. 1.

A 20-W, 879-nm, fibre-coupled (100 μm core diameter, 0.22 NA) laser diode was used to pump the resonator, and its output was focussed to a spot diameter of 300 μm which was incident on a 13-mm-long a-cut, Nd:GdVO$_4$ self-Raman crystal. The crystal had a clear aperture of 4 × 4 mm and was mounted in a water-cooled copper block. The input face of the crystal was coated high reflecting (HR) from 1063 to 1180 nm ($R > 99.99$ %) and anti-reflecting (AR) from 808 to 880 nm ($R < 0.1$ %); this coating acted as the input mirror ($M1$) of the resonator. The other face of the crystal was AR coated from 1063 to 1180 nm ($R < 0.01$ %). Mirror $M2$ had a radius of curvature of 300 mm and was HR coated from 1063 to 1180 nm ($R > 99.999$ %—manufacturer specified). A 4 × 4 array of spots (regions in which the HR coating was removed to the level of the mirror substrate) with diameters ranging from 20 to 120 μm was laser micro-machined into this mirror. The mirror was mounted on an x–y translation stage to allow its position to be adjusted, and enable oscillation of the laser centred on each of these spots, to test which spot produced an LG$_{01}$ mode.

A type I, non-critically phase-matched lithium triborate (LBO) crystal with dimensions 4 × 4 × 5 mm was used to perform SFG of the fundamental and Stokes fields. This crystal was mounted in a copper block and maintained at a temperature of 95 °C using a resistive heater.
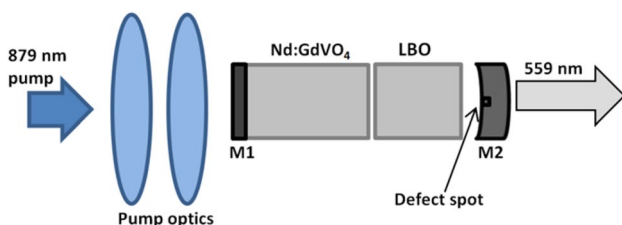
Fig. 1 Schematic of the experimental set-up

The spatial profile of the laser emission at the fundamental (1063 nm) and Stokes (1173 nm) wavelengths, along with the SFG (559 nm) wavelength, were examined using two CCD cameras (Spiricon-SP620U and COHU-4812). The topological charge of the vortex beams was examined using a Mach–Zehnder interferometer, the details of which can be found in [12, 22].

3 Results and discussion

3.1 Fundamental and Stokes fields

The resonator produced both the fundamental and Stokes fields as LG$_{01}$ modes (confirmed through interferometric analysis of the topological charge and the spatial profile) by using an overall cavity length of 28 mm and a mirror ($M2$) damage spot of diameter 40 μm. This yielded a damage spot to cavity mode ratio of 0.15, consistent with that in [21]. The laser was first examined without the intracavity LBO crystal. In this case, the topological charge of the fundamental and Stokes fields was stable and remained unchanged for timescales of minutes. Both fields always had identical sign of topological charge (+1 or −1), and the sign of this charge could only be altered by changing the resonator alignment. It is interesting to note that the level of stability of the fundamental and Stokes fields we observed in this work was similar to that observed in our prior work, where a resonator with a lower Q was used [12].

Threshold for generation of the fundamental and Stokes fields was achieved at incident pump powers of 0.3 and 1.1 W, respectively. The high reflectivity of the mirror $M2$, necessary to ensure high-intensity intracavity fields for SFG, meant that the output powers at 1063 and 1173 nm were low.

3.2 SFG field

With the LBO crystal placed intracavity, and temperature tuned for SFG of the fundamental and Stokes fields, significant fluctuation of the intensity of the SFG field was observed. Also, in contrast to the system without the LBO crystal, fluctuation of the fundamental and Stokes fields was also observed in both their spatial profile and topological charge. In spite of this fluctuation, it was still possible to power-scale the SFG emission; this is shown in Fig. 2. Note that the SFG power was as collected through output coupler ($M2$) only; SFG emission was also produced in the direction of the pump diode. The error bars are indicative of the level of fluctuation that was observed within the system.
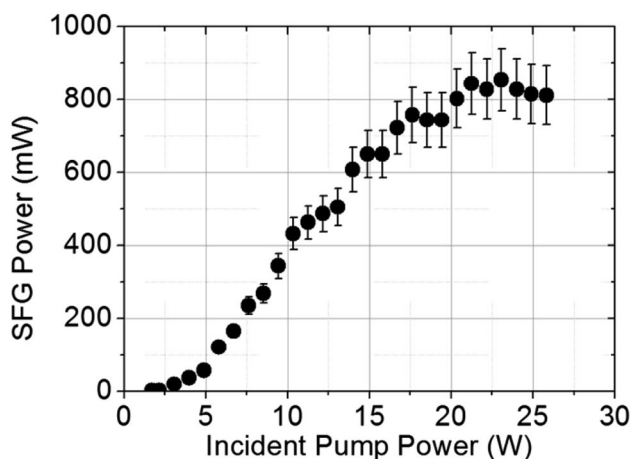
Fig. 2 Power scaling the SFG field

The beam quality factor (M^2) of the fundamental, Stokes, and SFG fields was measured. Near threshold, at an incident pump power of 3 W, the fundamental and Stokes fields exhibited an M^2 of 2.4, while the SFG field exhibited an M^2 of 3.6. As the incident pump power increased, the beam quality of the fundamental field degraded and, at maximum incident pump power, exhibited a value of 7.3. The Stokes field retained good beam quality (owing to Raman beam clean-up), with M^2 of 2.8, while the SFG field degraded, and had an identical value to the fundamental field. It should be noted that while the M^2 values of the fundamental and SFG fields were high, the spatial profiles still exhibited a central null region.

When examining the wavefront of the resonating NIR fields, it was found that the sign of the topological charge of the Stokes field was not always the same as that of the fundamental field. Raman gain is determined by the intensity profile and not the wavefront of the fundamental field; hence, it is possible for the Stokes field to lase with topological charge of $+1$ or -1. The sign of the topological charge of both the fundamental and Stokes fields was found to change temporally on the sub-1-s timescale, and this is in contrast to the system without the intracavity LBO crystal. In that case, the topological charge of both NIR fields was comparatively stable and had the same value as one another. This is also in contrast to the result observed when generating the second harmonic of the Stokes field [21]. As a consequence of this fluctuation, the topological charge of the SFG field also changed rapidly (also on the sub-1-s timescale), with values of $+2$ and 0 being observed with the interferometer. It was not possible to accurately determine the time frame on which this fluctuation occurred, due to the limited response time of the CCD camera. Images of the spatial profile of the SFG field in the near and far fields are shown in Fig. 3a, b, respectively, along

with interferograms taken in the near field, showing a topological charge of $+2$ and topological charge of 0 in Fig. 3c, d, respectively.

We speculate that the rapid fluctuation in the spatial profile and wavefront of the SFG and the NIR fields is due to competition between the two intracavity nonlinear effects of SRS and SFG. In this case, both the SRS and SFG processes act as simultaneous loss mechanisms for the fundamental field, and a balance between these losses cannot be maintained within the resonator, resulting in rapid fluctuations and flipping of the sign of topological charge of the NIR and consequently SFG fields. To further complicate matters, the resonator supports multiple longitudinal modes which begin to oscillate at higher incident pump powers and act to further increase the level of fluctuation. Further investigation of the fluctuation is required, and we plan to observe the temporal dynamics of the topological charge with the use of a fast detector such as a streak camera.

It is interesting to observe that the SFG field can exhibit a topological charge of $+2$ or 0 and yet retain an annular profile in the near field and a profile with a bright spot in the far field. The conditions under which a topological charge of $+2$ is observed and produces such near and far field profiles can be understood by the fundamental and Stokes fields having the same sign of topological charge (both $+1$). Similar to the theoretical investigation in [17], our theoretical model reveals that the different near and far field profiles manifest from a consideration of both Gouy phase which becomes relevant when frequency-mixing LG modes, and an additional phase component which develops within the resonator, as detailed in [21]. In contrast to the work in [17], our model very simply considers a decomposition of LG modes into Hermite–Gaussian modes and also considers the mixing of LG beams with the same and the opposite topological charge. The consideration of LG modes with opposite signs of topological charge ($+1$ and -1, respectively) was not detailed in [21]. A beam with a net topological charge of 0 should exhibit a Gaussian spatial profile in both the near and far fields. However, this is clearly not observed in this system. Here, we explicitly detail equations and simulations which consider the case where a SFG beam with topological charge of 0 is generated from a fundamental field with topological charge $+1$ and a Stokes field with topological charge -1.

In our model, we first assume that the LG resonator modes for the fundamental and Stokes fields are comprised of Hermite–Gaussian (HG) modes, $HG_{1,0}$ and $HG_{0,1}$, where

$$HG_{1,0} = xe^{-(x^2+y^2)} \tag{1}$$

$$HG_{0,1} = ye^{-(x^2+y^2)} \tag{2}$$

Fig. 3 Images of the spatial profile of the 559-nm SFG field in **a** the near field and **b** the far field. Interferogram images taken in the near field showing topological charge of **c** +2 and **d** 0
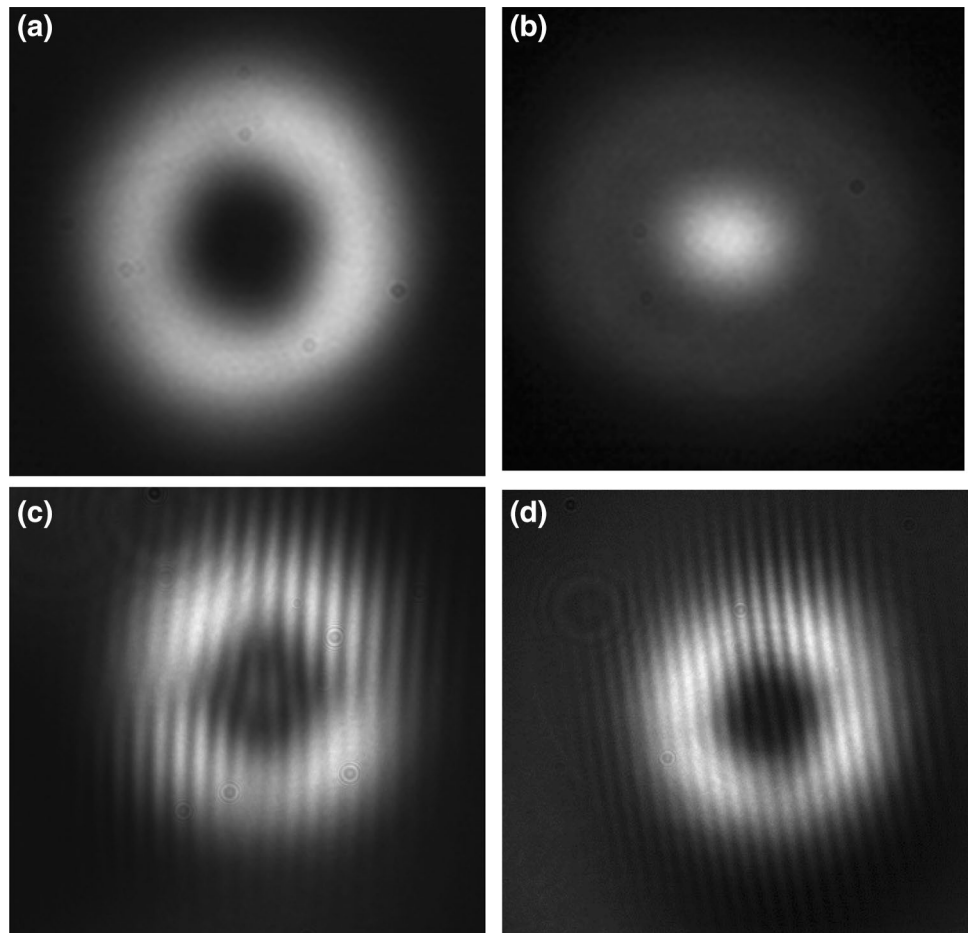
The expressions for the Laguerre–Gaussian vortex beams of the fundamental field with frequency (ω_1) and the Stokes field with frequency (ω_2) are given by:

$$\mathrm{LG}_1^{\omega_1} = xe^{-(x^2+y^2)} + iye^{-(x^2+y^2)}e^{i\Delta_1}, \tag{3}$$

$$\mathrm{LG}_{\pm1}^{\omega_2} = xe^{-(x^2+y^2)} \pm iye^{-(x^2+y^2)}e^{i\Delta_2} \tag{4}$$

where Δ_1 and Δ_2 are small phase mismatch terms which can manifest within the resonator [20]. In the expression for the Stokes field, ±1 denotes that the Stokes field can take a topological charge value of $+1$ or -1.

The field strength of the sum frequency is given by:

$$\begin{aligned}E_{\mathrm{SFG}} &= \mathrm{LG}_1^{\omega_1} \cdot \mathrm{LG}_{\pm1}^{\omega_2} = \left(x^2 \mp y^2 e^{i(\Delta_1+\Delta_2)}\right)e^{-2(x^2+y^2)} \\ &\quad + i\left(e^{i\Delta_1} \pm e^{i\Delta_2}\right)xye^{-2(x^2+y^2)} \\ &= \mathrm{HG}_{2,0} \mp \mathrm{HG}_{0,2}e^{i(\Delta_1+\Delta_2)} + \frac{1}{2}\left(1 \mp e^{i(\Delta_1+\Delta_2)}\right)\mathrm{HG}_{0,0} \\ &\quad + i\left(e^{i\Delta_1} \pm e^{i\Delta_2}\right)\mathrm{HG}_{1,1}\end{aligned} \tag{5}$$

For HG modes, the Gouy phase term is represented as:

$$\delta_{m,n} = (m+n+1)\tan^{-1}\frac{z}{z_R} \tag{6}$$

thus,

$$\delta(z) = \delta_{2,0} - \delta_{0,0} = \delta_{0,2} - \delta_{0,0} = \delta_{1,1} - \delta_{0,0} = 2\tan^{-1}\frac{z}{z_R}$$

The intensity of the SFG field is given by

$$I_{\mathrm{SFG}}(z) = |E_{\mathrm{SFG}}|^2$$

$$\begin{aligned}I_{\mathrm{SFG}}(z) = \Big| &\mathrm{HG}_{2,0} \mp \mathrm{HG}_{0,2}e^{i(\Delta_1+\Delta_2)} \\ &+ \frac{1}{2}\left(1 \mp e^{i(\Delta_1+\Delta_2)}\right)\mathrm{HG}_{0,0}e^{i\delta(z)} \\ &+ i\left(e^{i\Delta_1} \pm e^{i\Delta_2}\right)\mathrm{HG}_{1,1}\Big|^2\end{aligned} \tag{7}$$

In the case of small phase mismatch,

$$\langle \sin\Delta_1 \rangle = \langle \sin\Delta_2 \rangle = \langle \sin(\Delta_1+\Delta_2) \rangle = 0$$

$$\langle 1 + \cos(\Delta_1+\Delta_2) \rangle = 2\langle 1 - \cos(\Delta_1+\Delta_2) \rangle = \frac{(\Delta_1+\Delta_2)^2}{2}$$

Fig. 4 Simulated intensity profile of the SFG field in **a** the near field ($z = 0$) and **b** the far field ($z = 5z_\mathrm{R}$), through solution of Eq. (8) for the case where the fundamental and Stokes beams have a topological charge of $+1$
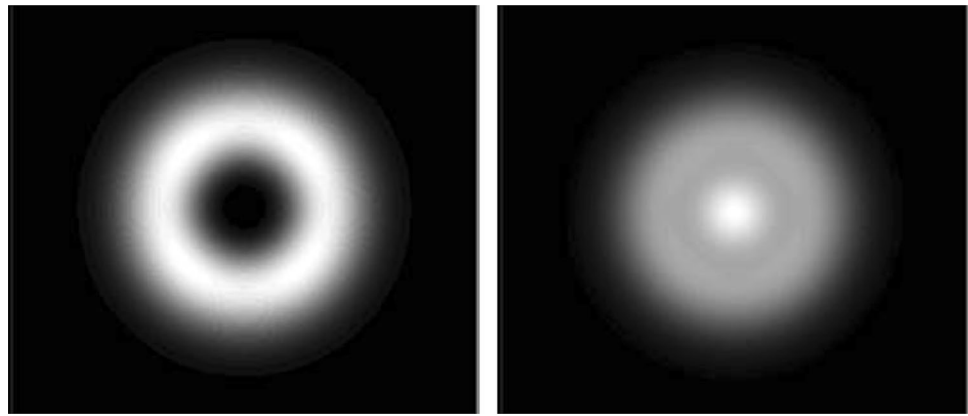
Fig. 5 Simulated intensity profile of the SFG field in **a** the near field ($z = 0$) and **b** the far field ($z = 5z_\mathrm{R}$), through solution of Eq. (9), for the case where the fundamental and Stokes fields have topological charge $+1$ and -1, respectively
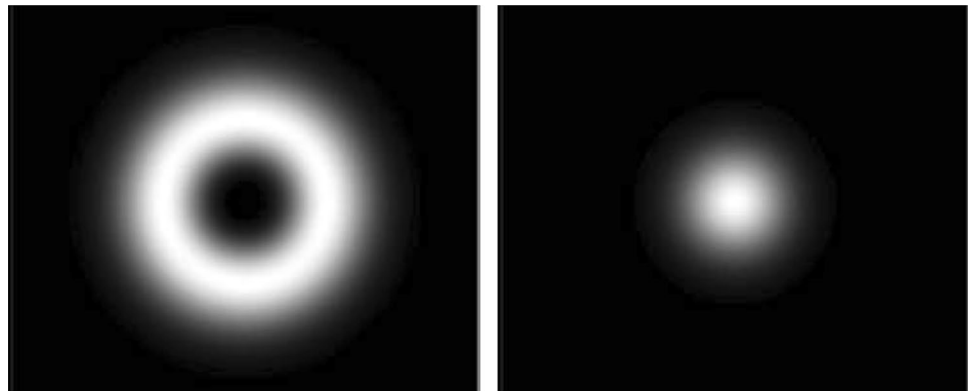
In the case where the fundamental and Stokes fields have the same sign of topological charge (i.e. both $+1$), the intensity of the resultant SFG field can be expressed as:

$$I_\mathrm{SFG}^{l=2}(z) = |\mathrm{HG}_{2,0}|^2 + |\mathrm{HG}_{0,2}|^2 + (\Delta_1 + \Delta_2)^2 |\mathrm{HG}_{0,0}|^2 + 4|\mathrm{HG}_{1,1}|^2$$
$$- 2\mathrm{HG}_{2,0}\mathrm{HG}_{0,2} + \frac{(\Delta_1 + \Delta_2)^2}{2} \cos\delta \left(\mathrm{HG}_{2,0} + \mathrm{HG}_{0,2}\right)\mathrm{HG}_{0,0} \tag{8}$$

In the case where the fundamental and Stokes fields have opposite sign of topological charge, the intensity of the resultant SFG field can be expressed as

$$I_\mathrm{SFG}^{l=0}(z) = \left|\mathrm{HG}_{2,0}\right|^2 + \left|\mathrm{HG}_{0,2}\right|^2 + \left|\mathrm{HG}_{0,0}\right|^2$$
$$- (\Delta_1 + \Delta_2)^2 \left|\mathrm{HG}_{1,1}\right|^2 + 2\mathrm{HG}_{2,0}\mathrm{HG}_{0,2}$$
$$+ 2\cos\delta \left(\mathrm{HG}_{2,0} + \mathrm{HG}_{0,2}\right)\mathrm{HG}_{0,0} \tag{9}$$

When we observe the spatial profile in the near field, z is small; hence, $\tan^{-1}\frac{z}{z_R} \to 0$. In the case where we observe the spatial profile in the far field, $\tan^{-1}\frac{z}{z_R} \to \frac{\pi}{2}$. We can then form explicit expressions for the intensity of the SFG fields in the near and far fields following both Eqs. (8) and (9). We simulated the spatial profiles in the near and far fields assuming a small phase mismatch parameter ($\Delta_1 = \Delta_2 = \frac{\pi}{25}$) and taking $z = 5z_\mathrm{R}$ to represent the far field. Th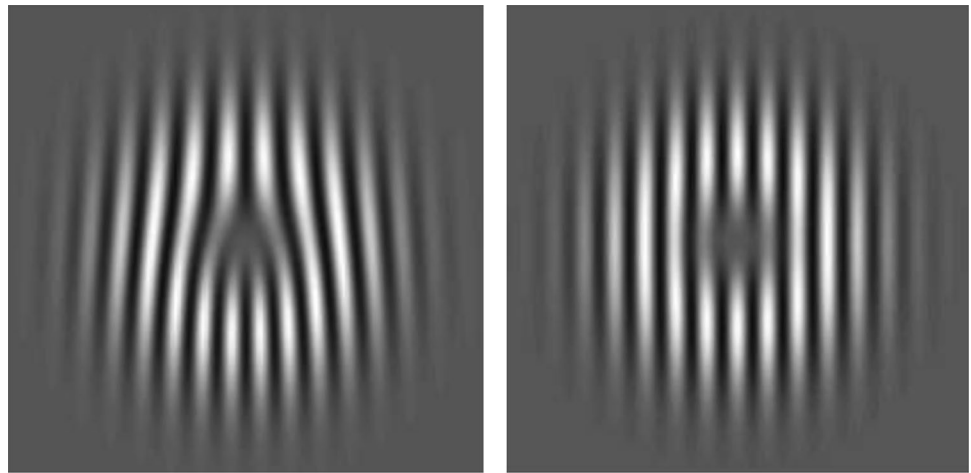e resultant spatial profiles for the case where the fundamental and Stokes have the same topological charge, and the case where they have opposite topological charge are shown in Figs. 4 and 5, respectively.

The simulated profiles in the near and far fields under the two combinations of topological charge are very similar in that an annular profile is observed in the near field and a central bright spot is observed in the far field. This is also consistent with the experimental observations shown in Fig. 3a, b. The simulations show that despite the topological charge of the fundamental and Stokes fields being opposite, the spatial profile of the SFG field retains an annular profile in the near field. We also simulated the interference pattern generated by the sum frequency field, in the near field, for the case where the fundamental and Stokes fields have the same topological charge, and the case where they have opposite topological charge. These are shown in Fig. 6a, b, respectively.

The simulated interference patterns for the SFG field are consistent with the experimental results in that when both the fundamental and Stokes fields have a topological charge of $+1$, we observe an SFG field with fringes consistent with a topological charge $+2$. Similarly in the case where the fundamental and Stokes fields have opposite topological charge of $+1$ and -1, we observe an SFG field with fringes consistent with a topological charge of

Fig. 6 Simulated interference pattern of the SFG field in the near field, for the case where **a** fundamental and Stokes fields have the same topological charge (+1 and +1) and **b** fundamental and Stokes fields have opposite topological charge (+1 and −1)

0. It demonstrates that in this system, under the process of SFG, conservation of topological charge is observed, but the resultant spatial profile of a field with net topological charge of 0 is not Gaussian. In our particular system, this has been supported by theory that includes an additional, small phase components which manifests between the HG modes which constitute the LG_{01} modes within the cavity. This result is significant as it highlights that the spatial profile of a vortex beam which is generated intracavity via SFG, despite carrying net topological charge of 0, can still retain an annular spatial profile in the near field.

We are currently exploring methods by which the stability of the topological charge of the Stokes and SFG fields can be maintained and controlled within the system. We believe that reducing the number of competing longitudinal modes within the cavity by way of intracavity etalons [23] will improve the stability of the system.

4 Conclusion

In this work, we have demonstrated sum frequency mixing of vortex beams within a self-Raman laser in a linear configuration. We observe fluctuation of the intensity and topological charge of the SFG field, and the topological charge of the constituent near-infrared fundamental and Stokes fields. The non-Gaussian profile of the SFG field in near and far fields under condition of zero topological charge is explained via theoretical modelling, and the manifestation of additional, small phase components within the laser resonator.

References

1. D.G. Grier, A revolution in optical manipulation. Nature **424**, 810 (2003)
2. S. Franke-Arnold, L. Allen, M. Padgett, Advances in optical angular momentum. Las. Photon. Rev. **2**, 299 (2008)
3. K. Toyoda, K. Miyamoto, N. Aoki, R. Morita, T. Omatsu, Using optical vortex to control the chirality of twisted metal nanostructures. Nano Lett. **12**, 3645 (2012)
4. T. Omatsu, K. Chujo, K. Miyamoto, M. Okida, K. Nakamura, N. Aoki, R. Morita, Metal microneedle fabrication using twisted light with spin. Opt. Express **18**, 17967 (2010)
5. M. Watabe, G. Juman, K. Miyamoto, T. Omatsu, Light induced conch-shaped relief in an azo-polymer film. Sci. Rep. **4**, 4281 (2014)
6. S.W. Hell, J. Wichmann, Breaking the diffraction resolution limit by stimulated emission: stimulated-emission-depletion fluorescence microscopy. Opt. Lett. **19**, 780 (1994)
7. L. Allen, S.M. Barnett, M.J. Padgett, *Optical Angular Momentum* (Institute of Physics, Bristol, 2003)
8. V.V. Kotlyar, A.A. Almazov, S.N. Khonina, V.A. Soifer, H. Elfstrom, J. Turnen, Generation of phase singularity through diffracting a plane or Gaussian beam by a spiral phase plate. J. Opt. Soc. A **22**, 849 (2005)
9. N. Matsumoto, T. Ando, T. Inoue, Y. Ohtake, N. Fukuchi, T. Hara, Generation of high-quality higher-order Lagurre-Gaussian beams using liquid-crystal-on-silicon spatial light modulators. J. Opt. Soc. A **25**, 1642 (2008)
10. F. Flossmann, U.T. Schwarz, M. Maier, Propagation dynamics of optical vortices in Laguerre–Gaussian beams. Opt. Commun. **250**, 218 (2005)
11. K. Kano, Y. Kozawa, S. Sato, Generation of purely single transverse mode vortex beam from a He–Ne laser cavity with a spot-defect mirror. Int. J. Opt. **2012**, 359141 (2012)
12. A.J. Lee, T. Omatsu, H.M. Pask, Direct generation of a first-Stokes vortex laser beam from a self-Raman laser. Opt. Express **21**, 12401 (2013)
13. M. Okida, T. Omatsu, M. Itoh, T. Yatagai, Direct generation of high power Laguerre–Gaussian output from a diode-pumped Nd:YVO$_4$ 1.3 µm bounce laser. Opt. Express **15**, 7616 (2007)
14. J.-F. Bisson, Y. Senatsky, K.-I. Ueda, Generation of Laguerre–Gaussian modes in Nd:YAG laser using diffractive optical pumping. Laser Phys. Lett. **2**, 327 (2005)
15. M. Padgett, L. Allen, Light with a twist in its tail. Contemp. Phys. **41**, 275 (2000)

16. K. Dholakia, N.B. Simpson, M.J. Padgett, L. Allen, Second-harmonic generation and the orbital angular momentum of light. Phys. Rev. A **54**, R3742 (1996)

17. Y.C. Lin, K.F. Huang, Y.F. Chen, The formation of quasi-non-diffracting focused beams with second-harmonic generation of flower Laguerre–Gaussian modes. Laser Phys. **23**, 115405 (2013)

18. M. Martinelli, J.A.O. Huguenin, P. Nussenzveig, A.Z. Khoury, Orbital angular momentum exchange in an optical parametric oscillator. Phys. Rev. A **70**, 013812 (2004)

19. K. Miyamoto, S. Miyagi, M. Yamada, K. Furuki, N. Aoki, M. Okida, T. Omatsu, Optical vortex pumped mid-infrared optical parametric oscillator. Opt. Express **19**, 12220 (2011)

20. K. Furuki, M.-T. Horikawa, A. Ogawa, K. Miyamoto, T. Omatsu, Tunable mid-infrared (6.3–12 μm) optical vortex pulse generation. Opt. Express **22**, 26351 (2014)

21. A.J. Lee, C. Zhang, T. Omatsu, H.M. Pask, An intracavity, frequency-doubled self-Raman vortex laser. Opt. Express **22**, 5400 (2014)

22. I.V. Basistiy, M.S. Soskin, M.V. Vasnetsov, Optical wavefront dislocations and their properties. Opt. Commun. **119**, 604 (1995)

23. G.M. Bonner, J. Lin, A.J. Kemp, J. Wang, H. Zhang, D.J. Spence, H.M. Pask, Spectral broadening in continuous-wave intracavity Raman lasers. Opt. Express **22**, 7492 (2014)